

Computation of Mixed-Mode Stress Intensity Factors for Cracks in Three-Dimensional Functionally Graded Solids

Matthew C. Walters¹; Glaucio H. Paulino²; and Robert H. Dodds Jr.³

Abstract: This work applies a two-state interaction integral to obtain stress intensity factors along cracks in three-dimensional functionally graded materials. The procedures are applicable to planar cracks with curved fronts under mechanical loading, including crack-face tractions. Interaction-integral terms necessary to capture the effects of material nonhomogeneity are identical in form to terms that arise due to crack-front curvature. A discussion reviews the origin and effects of these terms, and an approximate interaction-integral expression that omits terms arising due to curvature is used in this work to compute stress intensity factors. The selection of terms is driven by requirements imposed by material nonhomogeneity in conjunction with appropriate mesh discretization along the crack front. Aspects of the numerical implementation with (isoparametric) graded finite elements are addressed, and examples demonstrate the accuracy of the proposed method.

DOI: 10.1061/(ASCE)0733-9399(2006)132:1(1)

CE Database subject headings: Cracking; Three-dimensional analysis; Computation; Stress intensity factor.

Introduction

A significant body of experimental work has been performed to understand crack behavior in functionally graded materials (FGMs), and numerical methods have been developed to complement these experimental investigations, as well as to assist in the development of engineered FGM systems (e.g., Suresh and Mortensen 1998; Paulino et al. 2002). FGMs employed in applications such as thermal barrier coatings are exposed to severe stress gradients induced by thermal and/or mechanical loading. These harsh conditions frequently lead to the formation of surface cracks, which are a significant failure mechanism in FGM coatings (e.g., Choules et al. 2001; Rangaraj and Kokini 2003). Many works develop numerical techniques to analyze cracks in two-dimensional (2D) FGM specimens (e.g., Eischen 1987; Konda and Erdogan 1994; Gu et al. 1999; Anlas et al. 2000; Chan et al. 2001; Dag and Erdogan 2002; Dolbow and Gosz 2002; Kim and Paulino 2002a; Chan et al. 2003; Kim and Paulino 2003a; Huang

and Wang 2004; Kim and Paulino 2004), but few establish methods to analyze three-dimensional (3D) fractures such as the surface crack.

Analysis capabilities and understanding of 3D crack behavior in FGMs are improving, however. Ozturk and Erdogan (1995, 1996) solve integral equations to obtain stress intensity factors for axisymmetric cracks in infinite solids with a graded interface. Li and Zou (1998a,b) and Li et al. (1999) perform axisymmetric finite-element analyses of circumferentially cracked FGM cylinders. They compute mode-I stress intensity factors using a displacement correlation technique (DCT) which links computed crack-face displacements with Williams' (1957) stress-intensity-factor expressions for near-tip displacements. Jin et al. (2002, 2003) investigate quasistatic and elastic-plastic mode-I crack growth in 3D FGMs using a cohesive-zone model. Forth et al. (2003) simulate mixed-mode fatigue growth of surface cracks in FGMs using the DCT in conjunction with boundary-element analysis. Walters et al. (2004) use a form of the domain integral described by Shih et al. (1986), as well as the DCT, to compute mode-I stress intensity factors along surface cracks in FGM plates under thermal and mechanical loading. Jin and Dodds (2004) employ the same domain integral to investigate crack-growth-resistance behavior in 3D FGM specimens under mode-I loading. Established methods for computing mixed-mode stress intensity factors in 3D FGMs currently seem limited to the DCT (e.g., Forth et al. 2003). The present work investigates a robust and accurate, domain-based interaction-integral method for the computation of mixed-mode stress intensity factors along 3D cracks in FGMs.

Two-state interaction integrals are a powerful tool for the analysis of cracks under mixed-mode loading (Stern et al. 1976; Chen and Shield 1977). Interaction integrals involve numerical procedures similar to those necessary to evaluate the J -integral (e.g., Rice 1968; Yau et al. 1980) and are a convenient and accurate tool used widely to analyze cracks in 3D solids (e.g., Nakamura 1991; Dhondt 1998; Krysl and Belytschko 1999;

¹Dept. of Civil and Environmental Engineering, Univ. of Illinois at Urbana-Champaign, Newmark Civil Engineering Laboratory, 205 N. Mathews Ave., Urbana, IL 61801.

²Dept. of Civil and Environmental Engineering, Univ. of Illinois at Urbana-Champaign, Newmark Civil Engineering Laboratory, 205 N. Mathews Ave., Urbana, IL 61801 (corresponding author). E-mail: paulino@uiuc.edu

³Dept. of Civil and Environmental Engineering, Univ. of Illinois at Urbana-Champaign, Newmark Civil Engineering Laboratory, 205 N. Mathews Ave., Urbana, IL 61801.

Note. Associate Editor: Yunping Xi. Discussion open until June 1, 2006. Separate discussions must be submitted for individual papers. To extend the closing date by one month, a written request must be filed with the ASCE Managing Editor. The manuscript for this paper was submitted for review and possible publication on August 16, 2004; approved on March 14, 2005. This paper is part of the *Journal of Engineering Mechanics*, Vol. 132, No. 1, January 1, 2006. ©ASCE, ISSN 0733-9399/2006/1-1-15/\$25.00.

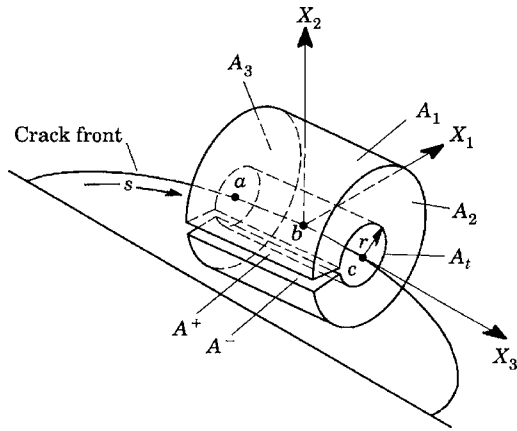


Fig. 1. Surfaces enclosing volume domain for computation of $J(s)$ at location $s=b$ along a curved crack front. For functionally graded material, A_r must shrink to the crack front, i.e., $r \rightarrow 0^+$.

Dhondt 2001, 2002; Wang 2004). Curvature of 3D crack fronts and crack surfaces imposes special requirements on the interaction-integral formulation. By including curvature effects, Nahta and Moran (1993); Gosz et al. (1998); and Gosz and Moran (2002) develop formulations of the interaction integral for axisymmetric cracks, curved 3D interface cracks, and nonplanar 3D cracks, respectively. Dolbow and Gosz (2002) extend the interaction-integral technique to FGMs by including additional terms to incorporate material gradients. Their work and subsequent studies employ interaction integrals to analyze cracks in 2D FGMs (e.g., Rao and Rahman 2003; Kim and Paulino 2003b,c,d; Paulino and Kim 2004). The present work extends existing capabilities to assess the significance of cracklike defects in FGMs by investigating the interaction-integral method as a tool for computing mixed-mode stress intensity factors along curved, planar 3D cracks in graded solids under mechanical loading.

The organization of the remaining sections is as follows: “Domain Integral for Three-Dimensional Cracks in Functionally Graded Materials” presents the domain integral that underlies the interaction integral employed in this study. “Interaction Integral for Three-Dimensional Cracks in Functionally Graded Materials” reviews the interaction-integral procedure for quasistatic, mechanical loading of FGMs, and “Numerical Aspects” describes related numerical procedures. “Numerical Examples” demonstrates the accuracy of interaction-integral computations for 3D FGMs through analyses of cracks in thin specimens under mixed-mode, in-plane loading, and of fully 3D specimens with cracks loaded in all three modes. Some observations conclude the work in “Discussion and Conclusions.”

Domain Integral for Three-Dimensional Cracks in Functionally Graded Materials

Shih et al. (1986) develop a domain integral to analyze 3D cracks in solids under thermomechanical loading including crack-face tractions. They derive an expression for $\bar{J}(s)$, the energy released by the unit advance of crack-front segment L_C , shown in Fig. 1. One form of this expression is

$$\bar{J}(s) = \int_V (\sigma_{ij}u_{j,1} - W\delta_{1i})q_{,i}dV + \int_V (\sigma_{ij}u_{j,1} - W\delta_{1i})_i q dV - \int_{A^+ + A^-} t_j u_{j,1} q dA \quad (1)$$

where stress components σ_{ij} , displacement derivatives $u_{j,1}$, crack-surface-traction components t_j , and the Kronecker delta δ_{ij} have Latin subscripts ranging from 1 to 3, and repeated indices imply summation. Strain energy density, W , for a linear-elastic material equals $(\sigma_{ij}\epsilon_{ij})/2$. The partial spatial derivative of (\cdot) , denoted by $(\cdot)_{,i} = \partial(\cdot)/\partial X_i$, is taken with respect to the X_i direction at position s of the local crack-front coordinate system illustrated in Fig. 1. Surfaces A^+ , A^- , A_1 , A_2 , A_3 , and A_r , also illustrated in Fig. 1, enclose volume V , which is free of singularities. For general loading conditions, surface A_r must shrink to the crack front (i.e., $r \rightarrow 0^+$). The scalar weight-function q varies smoothly within V , and enables transformation of the 2D J -integral into the 3D form presented in Eq. (1).

The second and third integrals in Eq. (1) vanish for quasistatic isothermal loading of elastic homogeneous materials with no body forces or crack-face tractions. The assumption that $\bar{J}(s)$ is nearly constant along crack segment L_C justifies approximating the pointwise energy release rate, $J(s)$, along a 3D crack front as (Shih et al. 1986)

$$J(s) = \frac{\bar{J}(s)}{\int_{L_C} q(s) ds} \quad (2)$$

Interaction Integral for Three-Dimensional Cracks in Functionally Graded Materials

Interaction integrals involve postprocessing steps after the solution of a boundary-value problem and require the superposition of actual, computed equilibrium fields, with fields from an auxiliary equilibrium state selected by the analyst. Evaluation of a conservation integral for this superimposed state leads to expressions that comprise interacting actual and auxiliary terms. Interaction integrals have been developed from Betti’s reciprocal theorem (Stern et al. 1976), the J -integral (Chen and Shield 1977), and the L - and M -integrals of Knowles and Sternberg (1972) (Choi and Earmme 1992; Kim et al. 2001). The present section describes an interaction-integral procedure to compute stress intensity factors along cracks in 3D FGMs under mechanical loading, and discusses terms that arise due to material nonhomogeneity and crack-front curvature.

Domain Integral for Two Superimposed Equilibrium States

For the equilibrium state represented by the superposition of actual and auxiliary fields, evaluation of the domain integral in Eq. (1) gives

$$\bar{J}^S(s) = \int_V \left[(\sigma_{ij} + \sigma_{ij}^{aux})(u_{j,1} + u_{j,1}^{aux}) - \frac{1}{2}(\sigma_{jk} + \sigma_{jk}^{aux})(\epsilon_{jk} + \epsilon_{jk}^{aux})\delta_{1i} \right] q_{,i} dV + \int_V \left[(\sigma_{ij} + \sigma_{ij}^{aux})(u_{j,1} + u_{j,1}^{aux}) \right]$$

$$\begin{aligned}
& - \frac{1}{2} (\sigma_{jk} + \sigma_{jk}^{aux}) (\varepsilon_{jk} + \varepsilon_{jk}^{aux}) \delta_{1i} \Big] q dV \\
& - \int_{A^+ + A^-} (t_j + t_j^{aux}) (u_{j,1} + u_{j,1}^{aux}) q dA \quad (3)
\end{aligned}$$

where superscripts *aux* and *S* indicate auxiliary and superimposed quantities, respectively. Eq. (3) separates into three components

$$\bar{J}^S(s) = \bar{J}(s) + \bar{J}^{aux}(s) + \bar{I}(s) \quad (4)$$

Here, $\bar{J}(s)$ is given by Eq. (1); $\bar{J}^{aux}(s)$ =domain integral comprising only auxiliary fields; and $\bar{I}(s)$ =integral of interacting actual and auxiliary terms

$$\begin{aligned}
\bar{I}(s) = & \int_V \left[\sigma_{ij} u_{j,1}^{aux} + \sigma_{ij}^{aux} u_{j,1} - \frac{1}{2} (\sigma_{jk} \varepsilon_{jk}^{aux} + \sigma_{jk}^{aux} \varepsilon_{jk}) \delta_{1i} \right] q_i dV \\
& + \int_V \left[\sigma_{ij} u_{j,1}^{aux} + \sigma_{ij}^{aux} u_{j,1} - \frac{1}{2} (\sigma_{jk} \varepsilon_{jk}^{aux} + \sigma_{jk}^{aux} \varepsilon_{jk}) \delta_{1i} \right] q dV \\
& - \int_{A^+ + A^-} t_j u_{j,1}^{aux} q dA \quad (5)
\end{aligned}$$

Eq. (5) assumes that auxiliary crack-face tractions are zero, and reduces further with the consideration of auxiliary fields, material gradients, and crack-front curvature.

Auxiliary Fields

A common approach to introduce stress intensity factors into the interaction integral is to define auxiliary fields according to the asymptotic fields near a crack (Williams 1957)

$$\sigma_{ij}^{aux} = \frac{K_I^{aux}}{\sqrt{2\pi r}} f_{ij}^I(\theta) + \frac{K_{II}^{aux}}{\sqrt{2\pi r}} f_{ij}^{II}(\theta) + \frac{K_{III}^{aux}}{\sqrt{2\pi r}} f_{ij}^{III}(\theta) \quad (6)$$

$$\begin{aligned}
u_j^{aux} = & \frac{K_I^{aux}}{2\mu(s)} \sqrt{\frac{r}{2\pi}} g_j^I[\theta, \nu(s)] + \frac{K_{II}^{aux}}{2\mu(s)} \sqrt{\frac{r}{2\pi}} g_j^{II}[\theta, \nu(s)] \\
& + \frac{2K_{III}^{aux}}{\mu(s)} \sqrt{\frac{r}{2\pi}} g_j^{III}[\theta, \nu(s)] \quad (7)
\end{aligned}$$

$$\varepsilon_{ij}^{aux} = \frac{1}{2} (u_{i,j}^{aux} + u_{j,i}^{aux}) \quad (8)$$

where r and θ =polar coordinates measured from the crack front; and $\mu(s)$ and $\nu(s)$ =respectively, the shear-modulus and Poisson-ratio values at crack-front location s . For convenience, Appendix I supplies expressions for the angular functions $f_{ij}(\theta)$ and the plane-stress and plane-strain forms for $g_j[\theta, \nu(s)]$. Eischen (1987) proves that the asymptotic crack-tip fields in materials with continuous, smooth gradients in material properties, are identical in form to those in homogeneous material given by Eqs. (6)–(8). Anlas et al. (2002) and Shim et al. (unpublished 2005) study the zone of dominance of these expressions in FGMs.

Influence of Material Gradients on the Interaction-Integral Formulation

The interaction integral for FGMs employed in this study follows the formulation proposed by Dolbow and Gosz (2002), which

compensates for material gradients through the definition of auxiliary strain components as the product of auxiliary stresses and the FGM compliance tensor, $S_{ijkl}(\mathbf{x})$ (see Appendix II)

$$\varepsilon_{ij}^{aux} = S_{ijkl}(\mathbf{x}) \sigma_{kl}^{aux} \quad (9)$$

Derivatives of auxiliary strain follow as

$$\varepsilon_{ij,1}^{aux} = S_{ijkl,1}(\mathbf{x}) \sigma_{kl}^{aux} + S_{ijkl}(\mathbf{x}) \sigma_{kl,1}^{aux} \quad (10)$$

Auxiliary stresses in Eq. (9) satisfy equilibrium, but strain-displacement compatibility is satisfied only with material properties at crack-front location s . For $\mathbf{x} \neq s$

$$\varepsilon_{ij}^{aux} = S_{ijkl}(\mathbf{x}) \sigma_{kl}^{aux} \neq \frac{1}{2} (u_{i,j}^{aux} + u_{j,i}^{aux}) \quad (11)$$

This incompatibility causes additional terms to appear in the interaction-integral formulation because

$$\sigma_{ij} (u_{j,1i}^{aux} - \varepsilon_{ij,1}^{aux}) \neq 0 \quad (12)$$

Rao and Rahman (2003) develop an alternative interaction integral for FGMs that employs a constant constitutive tensor for the auxiliary state. Paulino and Kim (2004) develop a third interaction integral for FGMs by defining auxiliary stresses as the product of the FGM constitutive tensor and auxiliary strains defined according to Eq. (8)

$$\sigma_{ij}^{aux} = C_{ijkl}(\mathbf{x}) \varepsilon_{kl}^{aux} \quad (13)$$

This definition causes the interaction integral to include additional terms because auxiliary stresses do not satisfy equilibrium at finite distances from the crack front, i.e., for $\mathbf{x} \neq s$

$$\sigma_{ij,i}^{aux} = (C_{ijkl}(\mathbf{x}) \varepsilon_{kl}^{aux})_{,i} \neq 0 \quad (14)$$

Influence of Crack-Front Curvature on the Interaction-Integral Formulation

Computation of r and θ values for the 2D auxiliary fields in Eqs. (6)–(8) occurs in planes normal to the crack front. For curved cracks, auxiliary fields must therefore be defined in curvilinear coordinates. Nahta and Moran (1993) observe that in a curvilinear coordinate system, the 2D auxiliary fields described by Williams' (1957) solution do not satisfy strain-displacement compatibility or stress equilibrium. Therefore

$$\sigma_{ij} (u_{j,1i}^{aux} - \varepsilon_{ij,1}^{aux}) \neq 0 \quad \text{and} \quad \sigma_{ij,i}^{aux} \neq 0 \quad (15)$$

For curved cracks, these nonvanishing terms appear in the interaction integral, and some auxiliary-field gradients also become nonzero [see Gosz et al. (1998)]. Thus both crack-front curvature and material nonhomogeneity bear similar influences on interaction-integral expressions. However, crack-front curvature requires the interaction integral to include *both* expressions in Eq. (15), whereas for two of the previously described interaction-integral formulations for FGMs, material nonhomogeneity requires *either* the expression in Eq. (12) *or* that in Eq. (14).

Interaction Integral for Curved Three-Dimensional Cracks in Functionally Graded Materials

An assumption of the interaction-integral procedure employed here is that all stress and strain components follow Hooke's law at any point within the solid, i.e.,

$$\sigma_{ij} = C_{ijkl}(\mathbf{x})\varepsilon_{kl} \quad \text{and} \quad \sigma_{ij}^{aux} = C_{ijkl}(\mathbf{x})\varepsilon_{kl}^{aux} \quad (16)$$

Eq. (16) leads to the relationships

$$\sigma_{ij}\varepsilon_{ij}^{aux} = C_{ijkl}(\mathbf{x})\varepsilon_{kl}\varepsilon_{ij}^{aux} = C_{klij}(\mathbf{x})\varepsilon_{ij}^{aux}\varepsilon_{kl} = \sigma_{ij}^{aux}\varepsilon_{ij} \quad (17)$$

which use a single constitutive tensor, $C_{ijkl}(\mathbf{x})$, to operate on both 3D actual fields and 2D auxiliary fields (see Appendix II). During the expansion of the second integral in Eq. (5), Eq. (17) permits writing actual stress derivatives as

$$\begin{aligned} \sigma_{ij,1}\varepsilon_{ij}^{aux} &= C_{ijkl,1}(\mathbf{x})\varepsilon_{kl}\varepsilon_{ij}^{aux} + C_{ijkl}(\mathbf{x})\varepsilon_{kl,1}\varepsilon_{ij}^{aux} \\ &= C_{ijkl,1}(\mathbf{x})\varepsilon_{kl}\varepsilon_{ij}^{aux} + \sigma_{ij}^{aux}\varepsilon_{ij,1} \end{aligned} \quad (18)$$

Finally, Eqs. (12), (15), (17), and (18) lead to the expression of Eq. (5) as

$$\begin{aligned} \bar{I}(s) &= \int_V (\sigma_{ij}u_{j,1}^{aux} + \sigma_{ij}^{aux}u_{j,1} - \sigma_{jk}\varepsilon_{jk}^{aux}\delta_{1i})q_{,i}dV \\ &+ \int_V [\sigma_{ij}(u_{j,1i}^{aux} - \varepsilon_{ij,1}^{aux}) + \underline{\sigma_{ij,i}^{aux}u_{j,1}} - C_{ijkl,1}(\mathbf{x})\varepsilon_{kl}\varepsilon_{ij}^{aux}]qdV \\ &- \int_{A^+A^-} t_{j,i}^{aux}q dA \end{aligned} \quad (19)$$

where equilibrium of actual stresses causes $\sigma_{ij,i}u_{j,1}^{aux}$ to vanish. For straight, traction-free cracks in homogeneous material, the second and third integrals of Eq. (19) vanish. For straight cracks in FGMs, the underlined terms in the second integral vanish, and for traction-free crack faces, Eq. (19) reduces to the interaction integral proposed by Dolbow and Gosz (2002). Kim (2003) and Paulino and Kim (2004) prove the existence of the interaction integral for FGMs by demonstrating that the second integral in Eq. (19) vanishes in the limit as the domain size shrinks to zero. A pointwise value of the interaction integral along a 3D crack front follows from the procedure in Eq. (2), i.e.

$$I(s) = \frac{\bar{I}(s)}{\int_{L_C} q(s)ds} \quad (20)$$

Extraction of Stress Intensity Factors

The energy release rate may be expressed as a function of the mixed-mode stress intensity factors K_I , K_{II} , and K_{III} (e.g., Anderson 1995)

$$J(s) = \frac{K_I^2 + K_{II}^2}{E^*(s)} + \frac{1 + \nu(s)}{E(s)}K_{III}^2 \quad (21)$$

where $E^*(s) = E(s)/[1 - \nu(s)^2]$ for plane-strain; and $E^*(s) = E(s)$ for plane-stress conditions. For FGMs, this expression requires material properties at crack-front location, s . From Eq. (21), superposition of actual and auxiliary states gives

$$\begin{aligned} J^S(s) &= \frac{1}{E^*(s)}[(K_I + K_I^{aux})^2 + (K_{II} + K_{II}^{aux})^2] + \frac{1 + \nu(s)}{E(s)}(K_{III} + K_{III}^{aux})^2 \\ &= J(s) + J^{aux}(s) + I(s) \end{aligned}$$

where

$$I(s) = \frac{1}{E^*(s)}(2K_I K_I^{aux} + 2K_{II} K_{II}^{aux}) + \frac{1 + \nu(s)}{E(s)}(2K_{III} K_{III}^{aux}) \quad (22)$$

Eqs. (19), (20), and (22) provide the necessary relationship between the interaction integral and actual stress intensity factors. By alternately assigning a nonzero value to each stress intensity factor, Eq. (22) yields

$$K_I(s) = \frac{E^*(s)}{2}I(s), \quad K_{II}(s) = \frac{E^*(s)}{2}I(s), \quad \text{and} \quad K_{III}(s) = \mu(s)I(s) \quad (23)$$

Numerical Aspects

Evaluation of the interaction integral using the finite-element method employs numerical techniques similar to those used to solve the boundary-value problem. This section provides a description of some relevant procedures. All computations in this study utilize *WARP3D*, a freely distributed, open-source finite-element code with extensive fracture-analysis capabilities, developed at the University of Illinois at Urbana-Champaign (Gullerud et al. 2004).

Numerical Evaluation of Volume and Surface Integrals

In a finite-element context, standard Gauss quadrature procedures permit the evaluation of Eq. (19) (e.g., Cook et al. 2002)

$$\begin{aligned} \bar{I}(s) &= \sum_V \sum_P^{elems \ gpts} [(\sigma_{ij}u_{j,1}^{aux} + \sigma_{ij}^{aux}u_{j,1} - \sigma_{jk}\varepsilon_{jk}^{aux}\delta_{1i})q_{,i} \det \mathbf{J}]_p w_p \\ &+ \sum_V \sum_P^{elems \ gpts} \{[\sigma_{ij}(u_{j,1i}^{aux} - \varepsilon_{ij,1}^{aux}) + \underline{\sigma_{ij,i}^{aux}u_{j,1}}] \\ &- C_{ijkl,1}(\mathbf{x})\varepsilon_{kl}\varepsilon_{ij}^{aux}\} q \det \mathbf{J}]_p w_p - \sum_S \sum_P^{faces \ gpts} (t_{j,i}^{aux}q \det \mathbf{J})_p w_p \end{aligned} \quad (24)$$

where the summations include all integration points on the interior or on the face of elements included in volume V . Weight w_p scales the function at each integration point, and $\det \mathbf{J}$ represents the determinant of the coordinate Jacobian for 2D surface or 3D volume coordinates. Here, the q -function follows the plateau variation described by Shih et al. (1986), quadrature over element volumes employs a $2 \times 2 \times 2$ rule, and quadrature for the surface integral in Eq. (19), which has a square-root singularity, follows the procedures in Walters et al. (2005).

Computation of Material-Property Derivatives

Numerical evaluation of Eq. (24) requires derivatives at element integration points of the compliance- and constitutive-tensor components. We interpolate specified nodal material properties $E(\mathbf{x})$ and $\nu(\mathbf{x})$ and compute their X_1 -derivatives at integration points using standard isoparametric interpolation (e.g., Li et al. 2000; Kim and Paulino 2002b):

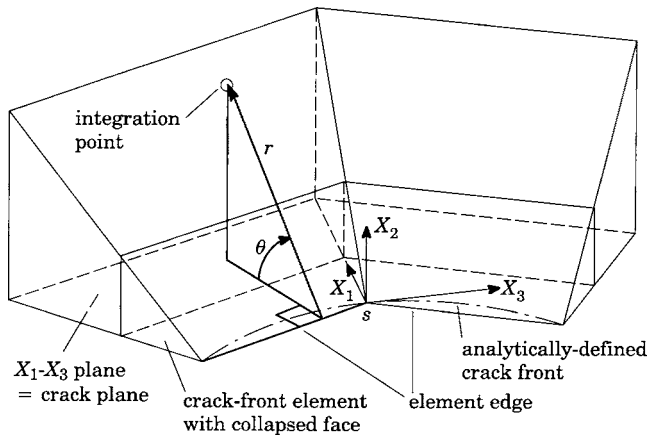


Fig. 2. Computation of r and θ for an integration point in a domain of four straight-edged elements. $I(s)$ values lead to stress intensity factors at crack-front location s .

$$[E(x)]_p = \sum_{I=1}^n N_I [E(x)]_I, \quad [E(x)_{,1}]_p = \sum_{I=1}^n \sum_{k=1}^3 \frac{\partial N_I}{\partial \eta_k} \frac{\partial \eta_k}{\partial X_1} [E(x)]_I \quad (25)$$

$$[v(x)]_p = \sum_{I=1}^n N_I [v(x)]_I, \quad \text{and} \quad [v(x)_{,1}]_p = \sum_{I=1}^n \sum_{k=1}^3 \frac{\partial N_I}{\partial \eta_k} \frac{\partial \eta_k}{\partial X_1} [v(x)]_I \quad (26)$$

where $[E(x)]_p$ and $[v(x)]_p$ denote material properties at integration points; n =number of element nodes; $[E(x)]_I$ and $[v(x)]_I$ =material properties at node I ; N_I =element shape function for node I evaluated at integration point p ; and η_k =parent coordinates. Integration-point values of $E(x)_{,1}$ and $v(x)_{,1}$ enable the direct computation of constitutive-tensor derivatives as

$$C_{ijkl}(x)_{,1} = \frac{\partial C_{ijkl}(x)}{\partial E(x)} E(x)_{,1} + \frac{\partial C_{ijkl}(x)}{\partial v(x)} v(x)_{,1} \quad (27)$$

where the quantities $\partial(\cdot)/E(x)$ and $\partial(\cdot)/v(x)$ denote explicit derivatives of (\cdot) with respect to $E(x)$ and $v(x)$. The same process yields $S_{ijkl}(x)_{,1}$.

Computation of r and θ for Auxiliary Fields

Auxiliary stresses and strains of order $O(r^{-1/2})$ are extremely sensitive to small errors in r when r is small. It is therefore important to compute r and θ values in curvilinear coordinates when crack-front elements have curved edges. Gosz et al. (1998) and Gosz and Moran (2002) provide thorough details for this procedure. For crack-front elements with straight edges, however, it is appropriate to compute r and θ using local Cartesian coordinates defined on each segment of the crack-front, as illustrated in Fig. 2 and discussed with more detail in Walters et al. (2005).

Numerical Examples

This section presents examples that include the computation of mode-I and mode-II stress intensity factors in thin, 3D FGM specimens under in-plane loading, as well as in fully 3D configurations.

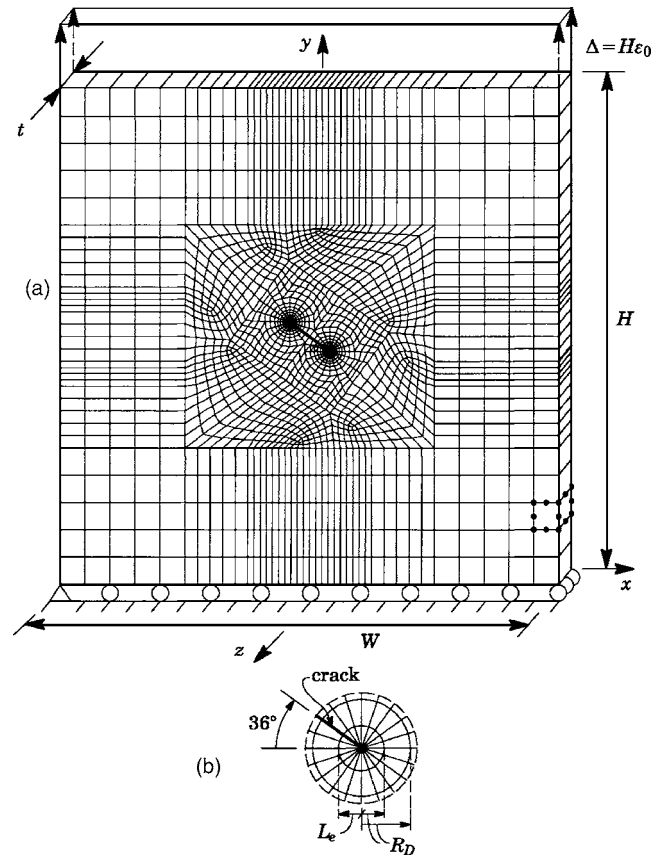


Fig. 3. (a) Mesh for fixed-grip displacement of a specimen with a crack inclined at 36° (see Table 1). Distance between crack fronts= $2a$. (b) Twenty collapsed crack-front elements of size $L_e/a=0.0177$ surround each crack front. Ratio R_D/a describes domain size in this work.

Three-Dimensional Analyses Simulating Plane-Stress and Plane-Strain Conditions

The interaction-integral procedure enables computation of stress intensity factors in thin 3D configurations under in-plane loading (e.g., Nakamura and Parks 1989; Wei et al. 2002). Analyses of a middle-crack tension specimen with an inclined crack permit useful observations regarding the simulation of plane-stress and plane-strain conditions with 3D FGM models. Fig. 3(a) shows a 3D mesh with a crack inclined at 36° , used to model this problem. A study of mesh-refinement levels for domain-integral computations in 2D FGMs is found in Kim and Paulino (2003d). In the present model, 20 elements with collapsed faces and quarter-point nodes surround the crack front as shown in Fig. 3(b). Length L_e indicates the size of the element adjacent to the crack front, and dimension R_D describes the radius of a domain of elements that surround the crack front. Model height H , width W , and thickness t have values relative to crack length $2a$ given by $H=W=20a$, and $t=0.125a$. Crack-front elements are of size $L_e/a=0.0177$. In this example, Young's modulus varies in the x direction as $E(x)=E_0 e^{\beta x}$, where $E_0=E(x=0)$, $\beta a=0.5$, and $\nu=0.3$. For loading, all nodes along $y=H$ have an imposed displacement $\Delta=H\epsilon_0$, where ϵ_0 =assigned strain value. For approximate plane-stress simulations, the model permits through-thickness deformations. Constrained through-thickness displacements impose plane-strain conditions.

Table 1. Normalized Stress Intensity Factors for In-Plane Displacement Loading of a Plate with a Through Crack Inclined at 36° (See Fig. 3)

Analysis	Source	K_{In} left	K_{In} right	K_{II_n} left	K_{II_n} right
Plane stress	Konda and Erdogan (1994)	0.460	0.925	-0.365	-0.548
	Present	0.446	0.902	-0.367	-0.556
	Present modified ^a	0.457	0.922	-0.362	-0.551
	Dolbow and Gosz (2002)	0.467	0.930	-0.364	-0.560
	Kim and Paulino (2003d)	0.456	0.922	-0.362	-0.551
Plane strain	Dong and Paulino (unpublished 2004)	0.457	0.923	-0.363	-0.550
	Present	0.504	1.02	-0.398	-0.605
	Dong and Paulino (unpublished 2004)	0.505	1.02	-0.399	-0.605

^a $\sigma_{33}\epsilon_{33,1}^{aux} \equiv 0$.

For simulated plane-stress conditions, the model employed here generates nonzero through-thickness stresses, σ_{33} , when $\nu \neq 0$. Williams' (1957) solution for plane-stress conditions therefore leads to a nonzero value for the gradient of through-thickness strain

$$\epsilon_{33,1}^{aux} = \left[-\frac{\nu(\mathbf{x})}{E(\mathbf{x})} (\sigma_{11}^{aux} + \sigma_{22}^{aux}) \right]_{,1} \neq 0 \quad (28)$$

Consequently, the product $\sigma_{33}\epsilon_{33,1}^{aux}$ appearing in the second integral of Eq. (19) introduces error into computed stress intensity factors for simulated plane-stress conditions. Two analyses demonstrate the potential significance of this error. The first analysis allows nonzero σ_{33} values caused by through-thickness Poisson contraction, and for the second analysis, $\sigma_{33}\epsilon_{33,1}^{aux} \equiv 0$. Table 1 lists normalized stress intensity factors computed for the left and right crack fronts in this model. Normalization of stress intensity factors follows

$$K_n = \frac{K}{E_0 \epsilon_0 \sqrt{\pi a}} \quad (29)$$

When $\sigma_{33}\epsilon_{33,1}^{aux} \equiv 0$, computed stress intensity factors compare well with those of Konda and Erdogan (1994); Dolbow and Gosz (2002); Kim and Paulino (2003d); and Dong and Paulino (unpublished, 2004). These results recommend assigning a zero value to the product $\sigma_{33}\epsilon_{33,1}^{aux}$ when Eq. (19) is used for 3D simulations of plane-stress configurations. Alternative formulations of the interaction integral for FGMs may not require such a modification [see, e.g., Rao and Rahman (2003); Paulino and Kim (2004)]. An analysis of the current model for plane-strain conditions leads to computed stress intensity factors that match closely the results obtained by Dong and Paulino (unpublished, 2004) (see Table 1).

Figs. 4(a and b) illustrate the influence of interaction-integral components $\bar{I}_1 - \bar{I}_4$ on computed stress intensity factors for this problem, where

$$\bar{I}_1 = \int_V (\sigma_{ij} u_{j,1}^{aux} + \sigma_{ij}^{aux} u_{j,1} - \sigma_{jk} \epsilon_{jk}^{aux} \delta_{1i}) q_{,i} dV \quad (30)$$

$$\bar{I}_2 = \int_V \sigma_{ij} (u_{j,1i}^{aux} - \epsilon_{ij,1}^{aux}) q dV \quad (31)$$

$$\bar{I}_3 = \int_V -C_{ijkl,1}(\mathbf{x}) \epsilon_{kl} \epsilon_{ij}^{aux} q dV \quad (32)$$

$$\bar{I}_4 = \int_{A^+ + A^-} -t_j u_{j,1}^{aux} q dA \quad (33)$$

The plots in Figs. 4(a and b) show relative contributions of these terms to computed values of $\bar{I}(s)$ for each of the domains surrounding the right crack tip. Influence of the FGM terms in Eq. (19) ($\bar{I}_2 + \bar{I}_3$) increases with domain size, thus maintaining the path independence of $\bar{I}(s)$. Percentages shown on the right of each plot indicate the relative contribution to $\bar{I}(s)$ of interaction-integral components for the largest domain of size $R_D/a = 1.0$.

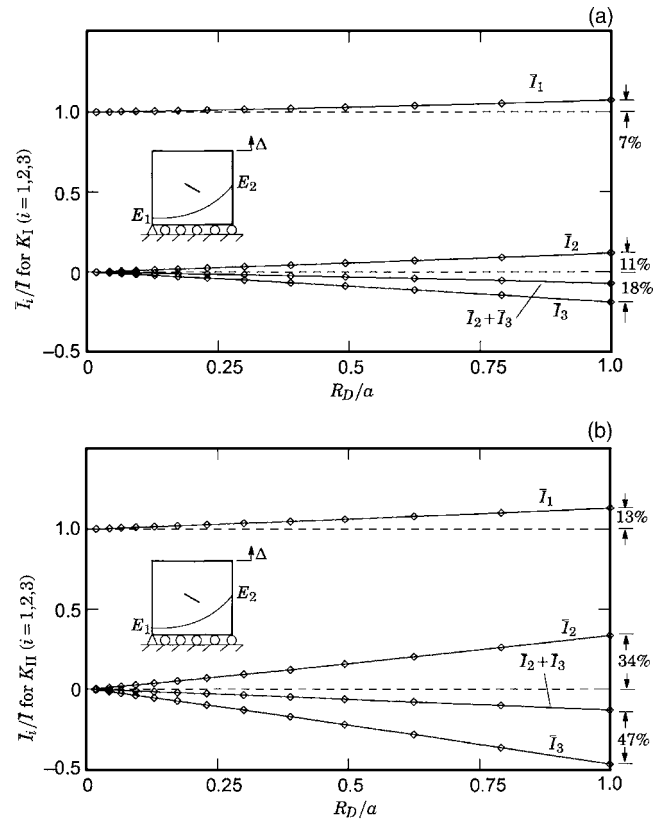


Fig. 4. Relative contribution of interaction-integral terms versus domain size for (a) K_I and (b) K_{II} for an inclined crack in an exponentially graded $M(T)$ specimen under plane-strain, fixed-grip loading.

Analysis of Planar, Curved Three-Dimensional Cracks in Functionally Graded Materials

This section examines four boundary-value problems involving mixed-mode loading of planar, curved cracks in FGMs. All examples in this section employ plane-strain auxiliary fields, with the assumption that near-plane-strain conditions exist near the crack front. Gosz et al. (1998) demonstrate that interaction-integral formulations incorporating the influence of crack-front curvature as described in “Auxiliary Fields” and “Interaction Integral for Curved Three-Dimensional Cracks in Functionally Graded Materials,” can greatly improve computed stress intensity factors for cracks in homogeneous and bimaterial specimens. Kim et al. (2001) also show differences between numerical results that employ and omit corrective terms due to crack curvature. Walters et al. (2005) show that for a variety of mixed-mode crack problems in homogeneous material, the influence of curvature terms depends significantly upon mesh discretization and becomes very small with mesh-refinement levels that permit accurate computation of J -integral values. In this study we omit all terms from the interaction integral procedure that arise solely from the influence of crack-front curvature. Omitted terms include those underlined in Eq. (19) and auxiliary-field quantities that reflect crack curvature (Gosz et al. 1998). This means that here, material nonhomogeneity dictates use of the terms in Eq. (12)—not crack-front curvature. Examples in this section demonstrate that good accuracy can be achieved using these approximations.

Mode-I and Mode-II Loading of a Penny-Shaped Crack in a Graded Interface

In this example, a penny-shaped crack with uniform opening pressure lies on the boundary of a graded interface. A semi-infinite solid with Young’s modulus E_1 occupies the half-space $z \leq 0$, and another half-space with modulus E_3 occupies the region $z \geq h$. A graded interfacial layer lying in the region $0 \leq z \leq h$ has a Young’s modulus described by $E_2(z) = E_1 e^{\beta z}$, $E_2(z=h) = E_3$. Poisson’s ratio remains constant at 0.3 throughout the body. Material properties at $z=0$ and $z=h$ are continuous, but material gradients are not. Theoretically, this violates the condition of the proof by Eischen (1987) that material gradients be differentiable. The finite-element solution and interaction integral are not affected by this discontinuity in material gradients, however, so the numerical solution obtained here is only a close approximation to the semi-analytical solution to this problem obtained by Ozturk and Erdogan (1996).

A cylindrical mesh with a penny-shaped crack shown in Fig. 5(a) comprises 16,480 20-noded brick elements. Cylinder height H and diameter D compare to crack radius a as $H/a = D/a = 80$. Fig. 5(b) shows the mesh near the crack front, and illustrates schematically the material variation. The cylinder is formed by 20 sectors of elements that surround the longitudinal axis, and the crack is surrounded by 24 sectors of elements, as shown in Fig. 5(b). Elements incident on the crack front have quarter-point nodes and collapsed faces, and are of size $L_e/a = 0.00129$. Two such meshes allow a comparison between interaction-integral results obtained using either straight-edged or curved quadratic elements along the crack front. At any location along the crack, the average of interaction-integral values computed for domains two through five produces stress intensity factors normalized as

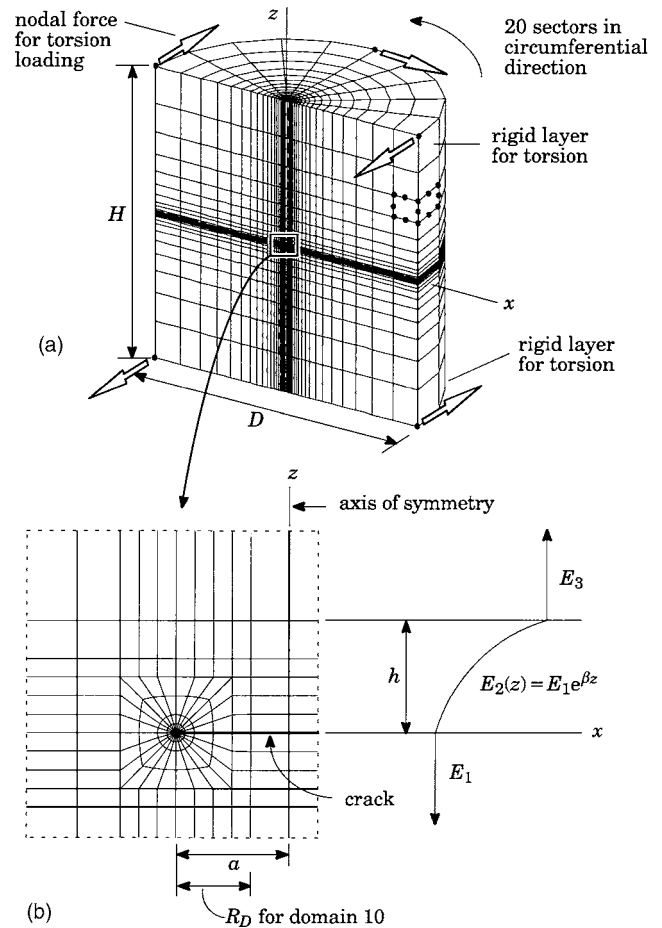


Fig. 5. (a) Mesh for infinite body with a penny-shaped crack on the boundary of a graded interfacial layer. (b) View of mesh in crack-front region showing schematic of material variation in interfacial layer for $h/a=1.0$. Twenty-four sectors of elements of size $L_e/a=0.00129$ surround the crack front.

$$K_n = \frac{K}{t_0 \sqrt{\pi a}} \quad (34)$$

where t_0 = magnitude of the crack-face traction. Table 2 lists present numerical results as well as stress intensity factors computed by Ozturk and Erdogan (1996) for different interfacial-layer thicknesses and material gradients. Stress intensity factor values obtained using curved crack-front elements are more accurate than those obtained from the mesh with straight crack-front segments despite the error introduced by inexact evaluation of the crack-face-traction integral in Eq. (19). For this crack configuration, accuracy of the numerical results depends heavily upon mesh refinement within and near the graded region, which in this example includes only three layers of elements for $h/a=0.5$ and five layers of elements for $h/a=1.0$ [see Fig. 5(b)]. Values in Table 2 agree well with Ozturk and Erdogan (1996) for moderate material gradients in the interfacial layer. A finer mesh discretization would permit computation of accurate results for more severe material gradients within the interfacial layer.

We now examine the effect of domain size on path independence of computed stress intensity factors for this problem, using the mesh with curved edges, in which element nodes lie on a circular crack front. For the homogeneous problem, normalized

Table 2. Normalized Stress Intensity Factors for a Penny-Shaped Crack at the Edge of a Graded Interface between Two Semi-Infinite Solids under Tension (See Fig. 5)

h/a	βa	E_3/E_1	Result	K_{In}	% difference	K_{II_n}	% difference
—	0.0	1.0	Ozturk and Erdogan (1996)	0.6366	—	—	—
			Straight edges	0.6299	-1.05	—	—
			Curved edges	0.6316	-0.79	—	—
0.5	0.5	1.28	Ozturk and Erdogan (1996)	0.6079	—	0.0149	—
			Straight edges	0.6035	-0.72	0.0146	-2.01
			Curved edges	0.6048	-0.51	0.0148	-0.67
1.0	0.5	1.65	Ozturk and Erdogan (1996)	0.5955	—	0.0201	—
			Straight edges	0.5913	-0.71	0.0196	-2.49
			Curved edges	0.5924	-0.52	0.0199	-1.0

K_I -values are compared with normalized K_I -values obtained from computed J -integral values using the plane-strain conversion

$$K_I = \sqrt{\frac{JE^*}{1-\nu^2}} \quad (35)$$

The ratio of the maximum domain size R_D , to crack radius a , is 0.66 for this problem. Fig. 6 illustrates a very small variation between the computed K_I -values for small and large domains, for the homogeneous case and the FGM case. This indicates that the effect of curvature terms omitted from Eq. (19) does not appear to change significantly within the range of domain sizes employed for this problem. Whether this trend holds for larger domains ($R_D/a > 1$) or for coarser meshes is uncertain.

The influence of FGM terms in Eq. (19) can be observed for this problem using the mesh with curved edges. Figs. 7(a and b) illustrate relative contributions to K_I and K_{II} from terms \bar{I}_1 – \bar{I}_4 in Eqs. (30)–(33). For mode-I computations, the FGM term \bar{I}_2 contributes roughly 2% for the largest domain, and the contribution from \bar{I}_3 is negligible, while the homogeneous term \bar{I}_1 and the crack-face-traction term \bar{I}_4 largely determine the computed K_I -value. For mode-II computations, \bar{I}_1 and \bar{I}_2 dominate, while \bar{I}_3 is negligible, and \bar{I}_4 is zero. The contribution from \bar{I}_3 for this problem is negligible because it involves the derivative of material gradients in the local X_1 direction, while the actual material gradient is in the X_2 direction.

In this example, \bar{I}_4 is nonzero only for mode-I interaction-integral computations, and therefore contributes no error to

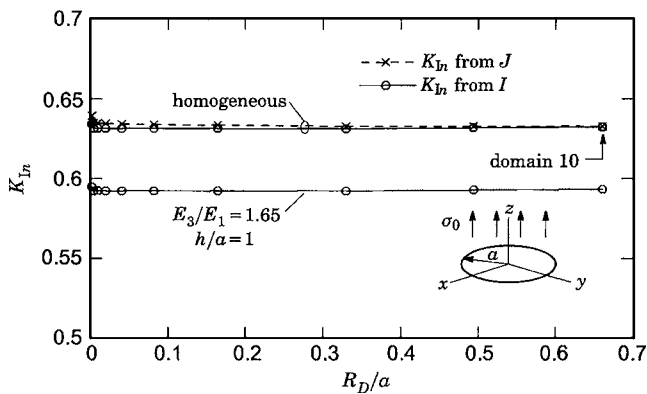


Fig. 6. Domain size R_D/a versus K_I due to crack-face pressure for the penny-shaped crack

the computed mode-II stress intensity factor. To evaluate the mode-I stress intensity factor K_I in this case, $K_I^{aux}=1.0$, and $K_{II}^{aux}=K_{III}^{aux}=0$. For $\theta = \pm\pi$, the integrand of \bar{I}_4 includes the product

$$t_{jI}^{aux} = \left[(0.0)(0.0) \pm \frac{t_2[\kappa(s)+1]}{4\mu(s)\sqrt{2\pi r}} + (0.0)(0.0) \right] \quad (36)$$

which includes the crack-surface traction, t_2 . For mode-II interaction-integral computations, $K_{II}^{aux}=1.0$, $K_I^{aux}=K_{III}^{aux}=0$, and the crack-face-traction integral includes

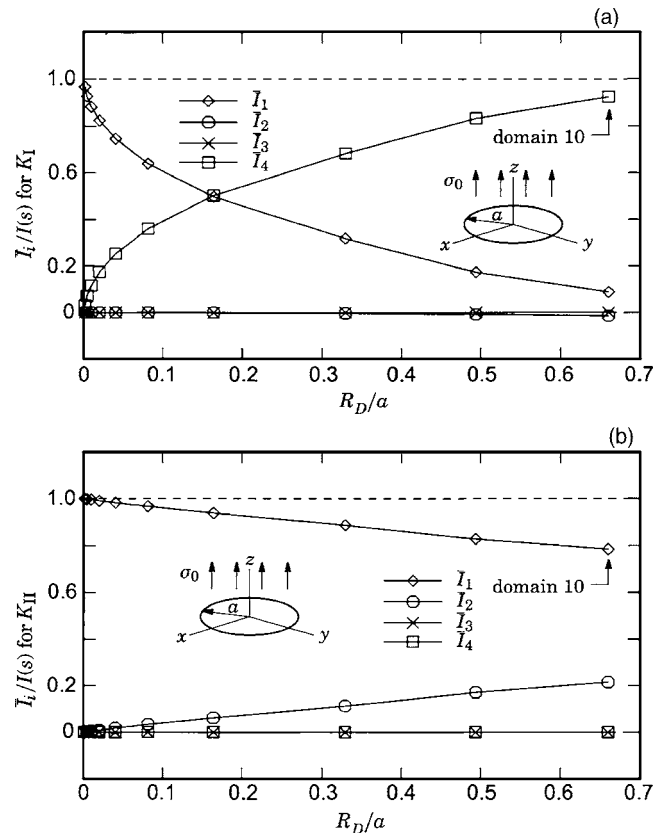


Fig. 7. Contributions to $I(s)$ from components I_1 – I_4 for a penny-shaped crack subjected to surface pressure in a graded interlayer ($h/a=1$, $E_3/E_1=1.65$) for (a) K_I and (b) K_{II} computations

Table 3. Normalized Stress Intensity Factors for a Penny-Shaped Crack at the Edge of a Graded Interface between Two Semi-Infinite Solids under Torsion (see Fig. 5)

h/a	E_3/E_1	Result	K_{III}	% difference
—	1.0	Ozturk and Erdogan (1995)	0.424	—
		Straight element edges	0.427	+0.71
		Curved element edges	0.419	-1.18
1.0	1/22	Ozturk and Erdogan (1995)	0.483	—
		Straight element edges	0.483	+0.0
		Curved element edges	0.475	-1.66
1.0	22	Ozturk and Erdogan (1995)	0.383	—
		Straight element edges	0.386	+0.78
		Curved element edges	0.379	-1.04
0.5	0.1	Ozturk and Erdogan (1995)	0.509	—
		Straight element edges	0.510	+0.20
		Curved element edges	0.501	-1.57
0.5	3.0	Ozturk and Erdogan (1995)	0.395	—
		Straight element edges	0.398	+0.76
		Curved element edges	0.390	-1.27

$$t_j u_{j,1}^{aux} = \left[\pm(0.0) \frac{[\kappa(s) + 1]}{4\mu(s)\sqrt{2\pi r}} \pm (t_2)(0.0) + (0.0)(0.0) \right] = 0 \quad (37)$$

meaning that the crack-surface-traction integral does not contribute to $\bar{I}(s)$ for mode-II computations, as witnessed in Fig. 7(b). The integrand of \bar{I}_4 for mode-III computations similarly vanishes for loading caused by t_2 . This example illustrates the fact that the surface-traction integral is nonzero only when crack-face tractions have a nonzero component in the direction of crack opening represented by the nonzero auxiliary stress intensity factor.

Mode-III Loading of a Penny-Shaped Crack in a Graded Interface

This third example of a 3D configuration demonstrates the accuracy of interaction-integral computations of mode-III stress intensity factors along cracks in a 3D FGM. The crack geometry, material variation, and finite-element meshes for this problem follow the descriptions in “Mode-I and Mode-II Loading...” and Fig. 5. Nodal loads at opposite ends of the cylinder apply torsion loading, and fixed nodes at the center of each cylinder face supply constraints [see Fig. 5(a)]. The element layer at each end of the cylinder is assigned a high value of Young’s modulus in order to ensure a uniform distribution of torsional stresses throughout the model.

At locations along the crack front where interaction-integral computations are performed, the average of stress intensity factors obtained from domains two through five is again the reported value. Normalization of the mode-III stress intensity factor follows Eq. (34), where $t_0 = 2Ta/\pi b^4$, in which T =total applied torque; and $b=D/2$ =cylinder radius. In the case of torsion applied through crack-face tractions, t_0 would be the magnitude of the traction at $r=a$.

Table 3 compares stress intensity factors computed for this problem with those obtained by Ozturk and Erdogan (1995), who solve integral equations for an axisymmetric crack with torsion applied to the crack faces. Computed stress intensity factors show

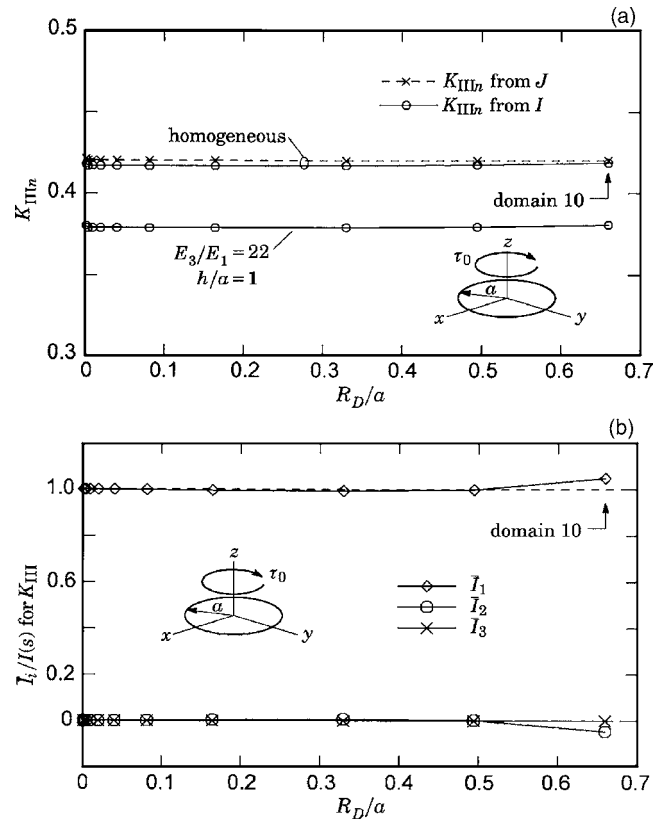


Fig. 8. (a) Domain size R_D/a versus K_{III} due to remote torsion for the penny-shaped crack in an infinite solid. (b) Component contributions to $I(s)$ for torsion of the penny-shaped crack, where $h/a=1$, and $E_3/E_1=22$.

excellent agreement with the semianalytical results even when material gradients are severe. For a similar material gradient, the mode-III problem shows very good accuracy compared to the mode-I, mode-II problem. This is likely due to the fact that for pure torsion, the governing equations of elasticity reduce to the Laplace equation, enabling a coarse mesh to approximate the solution more accurately. In this example, stress intensity factor values obtained using the mesh with straight element edges are more accurate than those obtained from the mesh with curved elements, which may be an effect of omitting crack-front curvature terms from the interaction integral.

Fig. 8(a) illustrates that the mesh with curved edges exhibits very good domain independence of computed stress intensity factors for mode-III. For the homogeneous and FGM cases, the two largest domains shown in Fig. 8(a) yield K_{III} -values that increase very slightly from values of smaller domains. This small variation may be due to the curvature terms omitted from Eq. (19) because a similar variation does not occur in normalized K_{III} -values obtained through J -integral computations according to

$$K_{III} = \sqrt{\frac{JE}{1+\nu}} \quad (38)$$

Contributions to computed K_{III} -values from individual components of Eq. (19) are illustrated in Fig. 8(b) for the mesh with curved edges. Once again, component \bar{I}_1 dominates the other terms. Term \bar{I}_2 contributes approximately 5% for the largest domain, and \bar{I}_3 is zero everywhere because the material

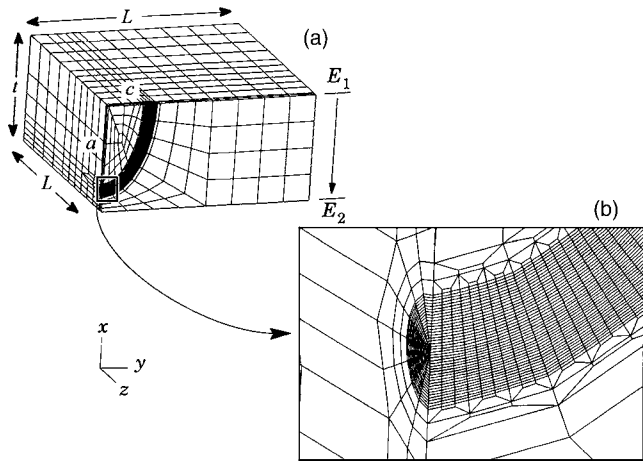


Fig. 9. (a) Quarter-symmetric mesh of semielliptical crack in plate under remote tension. (b) Detail of discretization in crack-front region.

gradient is in the X_2 direction. This example provides useful comparisons with a semianalytical solution, and demonstrates that good accuracy can be achieved when the interaction-integral formulation omits curvature terms. In the above example of a penny-shaped crack under tension and torsion loading, it is apparent that the strength and direction of the material gradient influences strongly the contribution of FGM terms in Eq. (19). A material gradient in the plane of the crack would engage the \bar{I}_3 term in Eq. (32). It is therefore useful to examine another 3D crack geometry in order to investigate the influence of all FGM terms in the presence of different material gradients.

Mode-I Loading of a Semielliptical Surface Crack in a Functionally Graded Material Plate

This analysis compares stress intensity factors obtained through interaction-integral and J -integral computations for a semielliptical surface crack in a functionally graded plate under remote tension. Symmetry of the problem permits reduction of the analysis model to one-quarter of the plate, discretized with a mesh of 13,556 20-noded hexagonal elements generated using *FEACrack* (2005) software [Fig. 9(a)]. Poisson's ratio is constant at 0.25, through-thickness gradients in Young's modulus vary according to $E(x) = E_1 e^{\beta x}$, $E_1 = E(x=0)$, $E_2 = E(x=t)$, and E_2/E_1

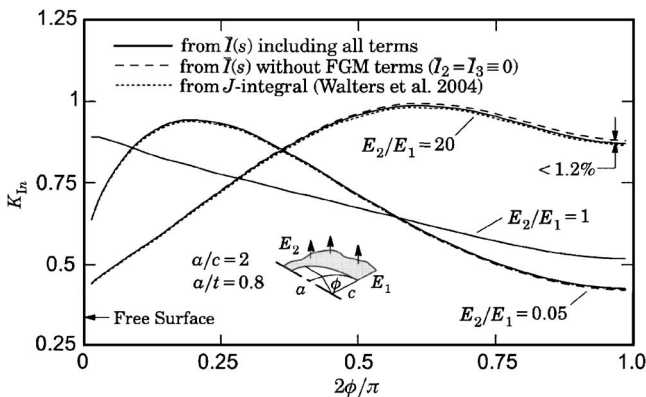


Fig. 10. Normalized K_I -values along a semielliptical surface crack in a Functionally Graded Material plate under remote tension

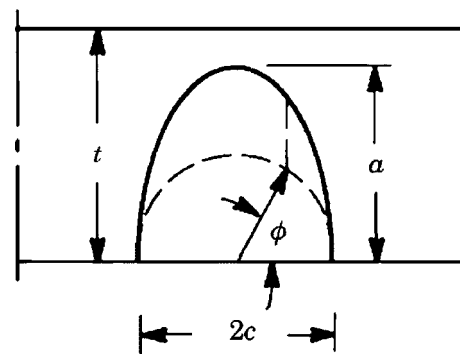


Fig. 11. Parametric angle ϕ indicates location along the semielliptical crack front

equals 0.05, 1, and 20. The ratio of crack width c to crack depth a is $a/c=2$, and the ratio of crack depth to plate thickness t is $a/t=0.8$. Other plate dimensions are $L=2t$. Fig. 9(b) shows mesh discretization in the crack-front region, where eight collapsed elements of size $L_e/a=0.00267$ surround the crack front. The high level of mesh refinement for this problem ensures good accuracy of computed J -integral and stress intensity factor values. Element edges along the crack front are straight, such that local crack-front curvature is zero, and computation of r and θ employs local Cartesian coordinates as described previously.

At each of 73 crack-front locations, 20 semicircular rings of elements enable computation of stress intensity factors using 20 different domains. Interaction-integral computations yield highly path-independent K_{In} -values, which, for nearly all crack-front locations, were identical up to four significant figures for domains 2–20. Standard normalization of stress intensity factors for elliptical cracks follows

$$K_{In} = \frac{K_I}{\sigma_0 \sqrt{\frac{\pi a}{Q}}} \quad (39)$$

where σ_0 =uniform remote tensile stress, and where Q may be approximated by

$$Q = 1 + 1.464 \left(\frac{c}{a} \right)^{1.65} \quad (40)$$

for $a/c > 1$ (Anderson 1995). Fig. 10 shows the variation along the crack of normalized stress intensity factor values obtained through Eq. (19). Parametric angle ϕ describes location along the crack front, as shown in Fig. 11. Plotted stress intensity fac-

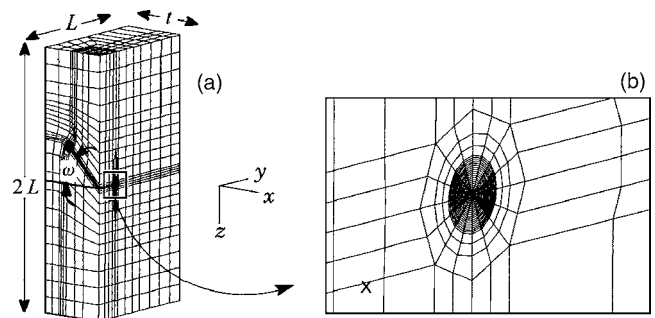


Fig. 12. (a) Mesh of semielliptical crack inclined at $\omega=45^\circ$ in plate under remote tension. (b) Detail of mesh in crack-front region.

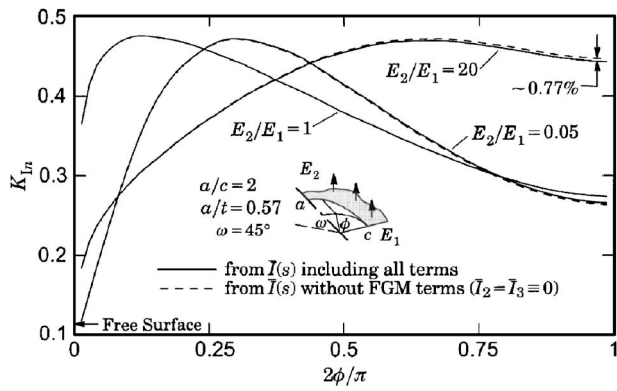


Fig. 13. Variation of K_{IIn} along front of inclined surface crack in plate under tension

tors compare with values obtained through a domain form of the J -integral for FGMs described by Walters et al. (2004). In this example, mesh refinement does not permit computations to reflect the true variation in stress intensity factor values near the free surface ($\phi=0^\circ$), where they decrease to zero within a small boundary layer (e.g., Pook 1994). Values for the domain at the free surface are therefore omitted from Fig. 10 and following plots. Due to inaccuracy of values computed using domains adjacent to the plane of symmetry ($\phi=90^\circ$), these values are also omitted from the following figures. Values computed using the J -integral and the interaction integral agree very closely, and for the homogeneous case, the plotted lines cannot be distinguished from one another—the maximum difference between data points being less than 0.1%. For all three cases of material variation, the maximum difference between the J -integral and interaction-integral curves is less than 0.75%. Fig. 10 also shows values of K_{IIn} computed using the interaction integral computed without the FGM terms \bar{I}_2 and \bar{I}_3 in Eqs. (31) and (32). Despite large material gradients in the FGM cases, the maximum contribution of these omitted terms for any data point occurs at the point closest to $\phi=90^\circ$, and is less than 1.2% of the total value. The difference between the interaction-integral curves with and without FGM terms becomes greatest toward $\phi=90^\circ$ because the exponentially varying material gradients are the steepest in that region.

Specimen and crack geometries may limit the domain size that can be employed practically for interaction-integral computations.

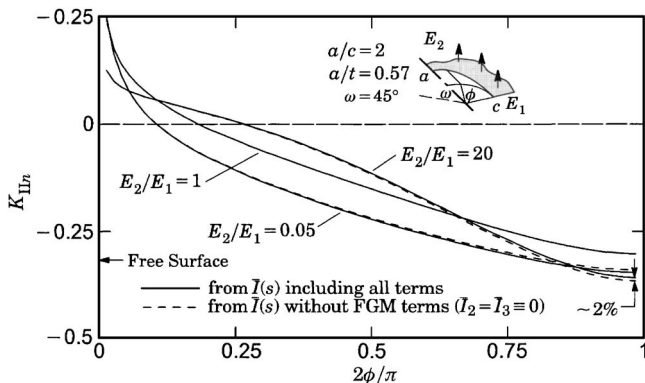


Fig. 14. Variation of K_{IIn} along front of inclined surface crack in plate under tension

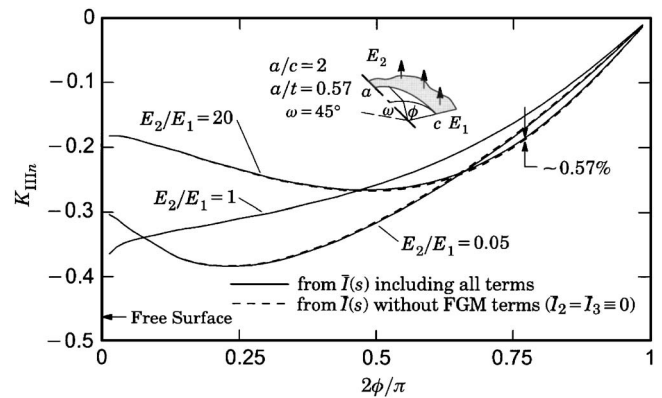


Fig. 15. Variation of K_{IIIn} along front of inclined surface crack in plate under tension

The largest domain employed in this example was of size $R_D/a=0.053$. This domain size can be compared to domain sizes shown in Figs. 4(a), 4(b), 7(a), 7(b), and 8(b), to give an idea of the expected contribution of FGM terms. In each of these example problems, the contribution of FGM terms is very small for the smallest domains. Fig. 10 illustrates that for mode-I loading of FGMs, a mesh with domain sizes that are small compared to the crack geometry yields stress intensity factors that do not depend significantly upon the FGM terms. This agrees with observations on J -integral computations in FGMs made by others such as Gu et al. (1999).

Mixed-Mode Loading of a Semielliptical Surface Crack in a Functionally Graded Material Plate

A final example illustrates the variation of computed stress intensity factors for a surface crack under mixed-mode loading. The plate geometry, crack aspect ratio, material variation, loading conditions, and mesh refinement level in the crack-front region are identical with those in the previous example in “Mode-I Loading of a Semielliptical...” In this example, however, the crack inclines at $\omega=45^\circ$ to the plate-thickness direction, as illustrated in Fig. 12(a). Therefore, though the ratio $a/c=0.8$ remains unchanged from the previous example, the inclined crack extends into the plate to a depth of $a/t=0.57$. *FEACrack* (2005) software again generated the mesh shown in Figs. 12(a and b). Excellent domain independence of computed stress intensity factors is

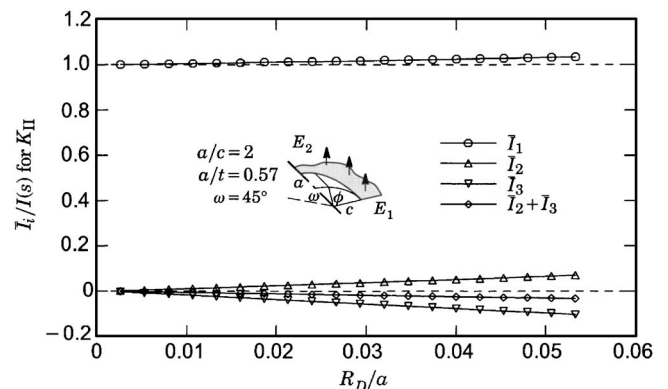


Fig. 16. Component contributions to $I(s)$ for K_{II} at $\phi=85^\circ$ along inclined surface crack in plate under tension where $E_2/E_1=20$

apparent at all interior locations along the crack, for each mode of loading and for each material variation. As in the previous example of a surface crack under mode-I loading, the small size of the domains with respect to the crack size limits the influence of the FGM terms \bar{I}_2 and \bar{I}_3 , as well as any potential influence of the omitted curvature terms. Figs. 13–15 show stress intensity factor values computed along the crack front for each mode of loading, both including and omitting the FGM terms. The maximum contribution of FGM terms occurs in the region of steepest material variation, yet represents a very small portion of the computed values in each case. Fig. 16 illustrates contributions of terms \bar{I}_1 – \bar{I}_3 for each of the 20 domains used to compute mode-II stress intensity factors at crack-front location $\phi=85^\circ$. Terms \bar{I}_2 and \bar{I}_3 are independently significant in the larger domains, but they largely cancel each other, making their combined contribution relatively small. This trend is very similar for the mode-I and mode-III computations for this problem, which are not shown here.

Discussion and Conclusions

This work examines interaction-integral procedures for planar, curved cracks in 3D functionally graded solids under remote mechanical loading and applied crack-face tractions. Computations omit auxiliary-field and interaction-integral terms that arise due to the effects of crack-front curvature. The excellent potential accuracy of computed stress intensity factors indicates that the influence of these terms is small for the problems considered, and that the proposed approach can provide very accurate stress intensity factors. The interaction-integral terms included to incorporate material gradients also contribute very little to stress intensity factor computations when the ratio of the domain size to the crack size is small. Figures such as 4(a and b) for simple 2D configurations might usefully indicate domain sizes for acceptably small error when domain integrals omit FGM terms.

Comparisons of computed stress intensity factors with existing semianalytical solutions demonstrate that the interaction integral is an accurate and useful tool for the analysis of cracks in 3D FGM configurations. Interaction-integral computations have been used with mesh-reduction techniques such as the boundary-element method (e.g., Sutradhar and Paulino 2004) and meshless methods (e.g., Krysl and Belytschko 1999), which have some advantages over finite-element analysis for simulation of crack propagation. Some of these methods might be employed to build on the work by Forth et al. (2003) to model crack growth in 3D FGMs. The anisotropy inherent to some FGM systems may also encourage the development of presented techniques to extend the work of Dhondt (2002) who employs the interaction-integral method to analyze anisotropic 3D specimens, and Kim and Paulino (2003c), who employ it for the analysis of 2D orthotropic FGM specimens. Interaction integrals developed to incorporate thermal-strain effects or to compute T -stresses in 3D FGMs are also at present unexplored.

Appendix I

Auxiliary Fields

Williams' (1957) solution for asymptotic stresses and displacements near the crack tip of a 2D specimen describe the auxiliary fields employed here (Anderson 1995)

$$\sigma_{11}^{aux} = \frac{1}{\sqrt{2\pi r}} \left[K_I^{aux} \cos \frac{\theta}{2} \left(1 - \sin \frac{\theta}{2} \sin \frac{3\theta}{2} \right) - K_{II}^{aux} \sin \frac{\theta}{2} \left(2 + \cos \frac{\theta}{2} \cos \frac{3\theta}{2} \right) \right] \quad (41)$$

$$\sigma_{22}^{aux} = \frac{1}{\sqrt{2\pi r}} \left[K_I^{aux} \cos \frac{\theta}{2} \left(1 + \sin \frac{\theta}{2} \sin \frac{3\theta}{2} \right) + K_{II}^{aux} \sin \frac{\theta}{2} \cos \frac{\theta}{2} \cos \frac{3\theta}{2} \right] \quad (42)$$

$$\sigma_{12}^{aux} = \frac{1}{\sqrt{2\pi r}} \left[K_I^{aux} \cos \frac{\theta}{2} \sin \frac{\theta}{2} \cos \frac{3\theta}{2} + K_{II}^{aux} \cos \frac{\theta}{2} \left(1 - \sin \frac{\theta}{2} \sin \frac{3\theta}{2} \right) \right] \quad (43)$$

$$\sigma_{13}^{aux} = -\frac{K_{III}^{aux}}{\sqrt{2\pi r}} \sin \frac{\theta}{2} \quad (44)$$

$$\sigma_{23}^{aux} = \frac{K_{III}^{aux}}{\sqrt{2\pi r}} \cos \frac{\theta}{2} \quad (45)$$

$$\sigma_{33}^{aux} = \begin{cases} \nu(s)(\sigma_{11}^{aux} + \sigma_{22}^{aux}) & \text{plane strain} \\ 0 & \text{plane stress} \end{cases} \quad (46)$$

$$u_1^{aux} = \frac{1}{2\mu(s)} \sqrt{\frac{r}{2\pi}} \left\{ K_I^{aux} \cos \frac{\theta}{2} \left[\kappa - 1 + 2 \sin^2 \frac{\theta}{2} \right] + K_{II}^{aux} \sin \frac{\theta}{2} \left[\kappa + 1 + 2 \cos^2 \frac{\theta}{2} \right] \right\} \quad (47)$$

$$u_2^{aux} = \frac{1}{2\mu(s)} \sqrt{\frac{r}{2\pi}} \left\{ K_I^{aux} \sin \frac{\theta}{2} \left[\kappa + 1 - 2 \cos^2 \frac{\theta}{2} \right] - K_{II}^{aux} \cos \frac{\theta}{2} \left[\kappa - 1 - 2 \sin^2 \frac{\theta}{2} \right] \right\}, \quad (48)$$

$$u_3^{aux} = \frac{K_{III}^{aux}}{\mu(s)} \sqrt{\frac{2r}{\pi}} \sin \frac{\theta}{2}, \quad (49)$$

where $\nu(s)$ and $\mu(s)$ =respectively, Poisson's ratio and the shear modulus at crack front location s , and

$$\kappa = \begin{cases} 3 - 4\nu(s) & \text{plane strain} \\ \frac{3 - \nu(s)}{1 + \nu(s)} & \text{plane stress} \end{cases} \quad (50)$$

Appendix II

Constitutive Relations

Constitutive models for an isotropic elastic material under isothermal mechanical loading couple stress components, σ_{ij} , to strain components, ε_{ij} , according to $\sigma_{ij} = \lambda \varepsilon_{kk} \delta_{ij} + 2\mu \varepsilon_{ij}$ (Fung 1965). Here, $i, j, k=1, 2, 3$, and the repeated index implies

summation. The symbol δ_{ij} =Kronecker delta; and $E=E(\mathbf{x})$ and $\nu=\nu(\mathbf{x})$ =Young's modulus and Poisson's ratio for the FGM. The Lamé parameters $\lambda(\mathbf{x})$ and $\mu(\mathbf{x})$ are

$$\lambda(\mathbf{x}) = \frac{\nu(\mathbf{x})E(\mathbf{x})}{[1 + \nu(\mathbf{x})][1 - 2\nu(\mathbf{x})]} \quad \text{and} \quad \mu(\mathbf{x}) = \frac{E(\mathbf{x})}{2[1 + \nu(\mathbf{x})]} \quad (51)$$

$$\begin{bmatrix} \sigma_{11} \\ \sigma_{22} \\ \sigma_{33} \\ \sigma_{12} \\ \sigma_{23} \\ \sigma_{13} \end{bmatrix} = \begin{bmatrix} \lambda(\mathbf{x}) + 2\mu(\mathbf{x}) & \lambda(\mathbf{x}) & \lambda(\mathbf{x}) & 0 & 0 & 0 \\ \lambda(\mathbf{x}) & \lambda(\mathbf{x}) + 2\mu(\mathbf{x}) & \lambda(\mathbf{x}) & 0 & 0 & 0 \\ \lambda(\mathbf{x}) & \lambda(\mathbf{x}) & \lambda(\mathbf{x}) + 2\mu(\mathbf{x}) & 0 & 0 & 0 \\ 0 & 0 & 0 & 2\mu(\mathbf{x}) & 0 & 0 \\ 0 & 0 & 0 & 0 & 2\mu(\mathbf{x}) & 0 \\ 0 & 0 & 0 & 0 & 0 & 2\mu(\mathbf{x}) \end{bmatrix} \begin{bmatrix} \varepsilon_{11} \\ \varepsilon_{22} \\ \varepsilon_{33} \\ \varepsilon_{12} \\ \varepsilon_{23} \\ \varepsilon_{13} \end{bmatrix} \quad (52)$$

where ε_{ij} =(symmetric) tensor-strain components. With appropriate definitions of strain components, Eq. (52) is valid for 3D actual fields, and 2D plane-stress and plane-strain auxiliary fields. Eq. (52) corresponds to plane stress when $\varepsilon_{33} \equiv \nu(\varepsilon_{11} + \varepsilon_{22}) / (\nu - 1)$, and $\varepsilon_{23} = \varepsilon_{13} \equiv 0$, and corresponds to plane strain when $\varepsilon_{33} = \varepsilon_{23} = \varepsilon_{13} \equiv 0$. Therefore, for isotropic elastic functionally graded material, the generalized Hooke's law for 3D actual and 2D auxiliary fields is

$$\sigma_{ij} = C_{ijkl}(\mathbf{x})\varepsilon_{kl} \quad \text{and} \quad \sigma_{ij}^{aux} = C_{ijkl}(\mathbf{x})\varepsilon_{kl}^{aux} \quad (53)$$

$$\begin{bmatrix} \varepsilon_{11}^{aux} \\ \varepsilon_{22}^{aux} \\ \varepsilon_{33}^{aux} \\ \varepsilon_{12}^{aux} \\ \varepsilon_{23}^{aux} \\ \varepsilon_{13}^{aux} \end{bmatrix} = \frac{1}{E(\mathbf{x})} \begin{bmatrix} 1 & -\nu(\mathbf{x}) & -\nu(\mathbf{x}) & 0 & 0 & 0 \\ -\nu(\mathbf{x}) & 1 & -\nu(\mathbf{x}) & 0 & 0 & 0 \\ -\nu(\mathbf{x}) & -\nu(\mathbf{x}) & 1 & 0 & 0 & 0 \\ 0 & 0 & 0 & 1 + \nu(\mathbf{x}) & 0 & 0 \\ 0 & 0 & 0 & 0 & 1 + \nu(\mathbf{x}) & 0 \\ 0 & 0 & 0 & 0 & 0 & 1 + \nu(\mathbf{x}) \end{bmatrix} \begin{bmatrix} \sigma_{11}^{aux} \\ \sigma_{22}^{aux} \\ \sigma_{33}^{aux} \\ \sigma_{12}^{aux} \\ \sigma_{23}^{aux} \\ \sigma_{13}^{aux} \end{bmatrix} \quad (54)$$

where ε_{ij}^{aux} are (symmetric) tensor-strain components. Appropriate stress definitions make Eq. (54) valid for 3D actual fields, and 2D plane-stress and plane-strain auxiliary fields. Eq. (54) corresponds to plane stress when $\sigma_{33}^{aux} = \sigma_{23}^{aux} = \sigma_{13}^{aux} \equiv 0$, and corresponds to plane strain when $\sigma_{33}^{aux} \equiv \nu(\sigma_{11}^{aux} + \sigma_{22}^{aux})$, and $\sigma_{23}^{aux} = \sigma_{13}^{aux} \equiv 0$. Therefore, for isotropic elastic functionally graded materials, the compliance relation for 3D actual and 2D auxiliary fields is

$$\varepsilon_{ij} = S_{ijkl}(\mathbf{x})\sigma_{kl} \quad \text{and} \quad \varepsilon_{ij}^{aux} = S_{ijkl}(\mathbf{x})\sigma_{kl}^{aux} \quad (55)$$

Formulations of the interaction integral for FGMs include the product $C_{ijkl,1}(\mathbf{x})\varepsilon_{kl}\varepsilon_{ij}^{aux}$. In this work, ε_{kl} denotes mechanical strain components for the actual 3D field, and ε_{ij}^{aux} denotes 2D plane-stress or plane-strain auxiliary fields corresponding to Williams' (1957) solution. For evaluation of this term as well as Eq. (17), it is convenient for the constitutive tensor $C_{ijkl}(\mathbf{x})$ to be identical for actual (3D) and auxiliary (2D) fields. The constitutive relationships may be expressed as

where the constitutive tensor $C_{ijkl}(\mathbf{x})$ is identical in both expressions. This permits the straightforward computation of $C_{ijkl,1}(\mathbf{x})\varepsilon_{kl}\varepsilon_{ij}^{aux}$ in Eq. (17).

The interaction-integral formulation used in this work defines strain components as the product of the compliance and auxiliary-stress tensors, $\varepsilon_{ij}^{aux} = S_{ijkl}(\mathbf{x})\sigma_{kl}^{aux}$. The compliance relations are $\varepsilon_{ij} = -\lambda\sigma_{kk}\delta_{ij} / [2\mu(3\lambda + 2\mu)] + 1/[2\mu]\sigma_{ij}$ (Fung 1965). Thus for auxiliary fields, the compliance relationships may be expressed as

Acknowledgments

The writers thank the support of the NASA Graduate Student Researchers Program (NGT 2-52271) and the NASA-Ames Engineering for Complex Systems Program (NAG 2-1424). Dr. Tina

Panontin at Ames serves as the technical monitor for these programs. The writers also gratefully acknowledge the National Science Foundation (NSF) Mechanics and Materials Program (CMS-0115954). The first writer wishes to thank Professor J.-H. Kim of the University of Connecticut for many helpful conversations, and the anonymous reviewers for useful suggestions. Any opinions, findings, conclusions, or recommendations expressed in this publication do not necessarily reflect the views of the sponsors.

References

- Anderson, T. L. (1995). *Fracture mechanics, fundamentals and applications*, 2nd Ed., CRC, New York.
- Anlas, G., Santare, M. H., and Lambros, J. (2000). "Numerical calcula-

- tion of stress intensity factors in functionally graded materials." *Int. J. Fract.*, 104, 103–143.
- Anlas, G., Santare, M. H., and Lambros, J. (2002). "Dominance of asymptotic crack tip fields in elastic functionally graded materials." *Int. J. Fract.*, 115, 193–204.
- Chan, Y.-S., Fannjiang, A. C., and Paulino, G. H. (2003). "Integral equations with hypersingular kernels—Theory and applications to fracture mechanics." *Int. J. Eng. Sci.*, 41, 683–720.
- Chan, Y.-S., Paulino, G. H., and Fannjiang, A. C. (2001). "The crack problem for nonhomogeneous materials under antiplane shear loading—A displacement based formulation." *Int. J. Solids Struct.*, 38, 2989–3005.
- Chen, F. H. K., and Shield, R. T. (1977). "Conservation laws in elasticity of the J-integral type." *Z. Angew. Math. Phys.*, 28, 1–22.
- Choi, N. Y., and Earmme, Y. Y. (1992). "Evaluation of stress intensity factors in a circular arc-shaped interfacial crack using *L*-integral." *Mech. Mater.*, 14, 141–153.
- Choules, B. D., Kokini, K., and Taylor, T. A. (2001). "Thermal fracture of ceramic thermal barrier coatings under high heat flux with time-dependent behavior—Part 1—Experimental results." *Mater. Sci. Eng., A*, 299, 296–304.
- Cook, R. D., Malkus, D. S., Plesha, M. E., and Witt, R. J. (2002). *Concepts and applications of finite element analysis*, Wiley, New York.
- Dag, S., and Erdogan, F. (2002). "A surface crack in a graded medium under general loading conditions." *ASME J. Appl. Mech.*, 69, 580–588.
- Dhondt, G. (1998). "On corner point singularities along a quarter circular crack subject to shear loading." *Int. J. Fract.*, 89, L33–L38.
- Dhondt, G. (2001). "3-D mixed-mode *K*-calculations with the interaction integral method and the quarter point element stress method." *Commun. Numer. Methods Eng.*, 17, 303–307.
- Dhondt, G. (2002). "Mixed-mode *K*-calculations in anisotropic materials." *Eng. Fract. Mech.*, 69, 909–922.
- Dolbow, J., and Gosz, M. (2002). "On the computation of mixed-mode stress intensity factors in functionally graded materials." *Int. J. Solids Struct.*, 39, 2557–2574.
- Eischen, J. W. (1987). "Fracture of nonhomogeneous materials." *Int. J. Fract.*, 34, 3–22.
- FEACrack 2.6; user's manual*. (2005). Structural Reliability Technology, 1898 South Flatiron Court, #235, Boulder, Colo. 80301.
- Forth, S. C., Favrow, L. H., Keat, W. D., and Newman, J. A. (2003). "Three-dimensional mixed-mode fatigue crack growth in a functionally graded titanium alloy." *Eng. Fract. Mech.*, 70, 2175–2185.
- Fung, Y. C. (1965). *Foundations of solid mechanics*, Prentice-Hall, Englewood Cliffs, N.J.
- Gosz, M., Dolbow, J., and Moran, B. (1998). "Domain integral formulation for stress intensity factor computation along curved three-dimensional interface cracks." *Int. J. Solids Struct.*, 35, 1763–1783.
- Gosz, M., and Moran, B. (2002). "An interaction energy integral method for computation of mixed-mode stress intensity factors along non-planar crack fronts in three dimensions." *Eng. Fract. Mech.*, 69, 299–319.
- Gu, P., Dao, M., and Asaro, R. J. (1999). "A simplified method for calculating the crack-tip field of functionally-graded materials using the domain integral." *ASME J. Appl. Mech.*, 66, 101–108.
- Gullerud, A., et al. (2004). *WARP3D Release 15 manual*, Civil Engineering, Rep. No. UILU-ENG-95-2012, Univ. of Illinois at Urbana-Champaign, Urbana, Ill.
- Huang, G.-Y., and Wang, Y.-S. (2004). "A new model for fracture analysis of a functionally graded interfacial zone under harmonic anti-plane loading." *Eng. Fract. Mech.*, 71, 1841–1851.
- Jin, Z.-H., and Dodds, R. H., Jr. (2004). "Crack growth resistance behavior of a functionally graded material: Computational studies." *Eng. Fract. Mech.*, 71, 1651–1672.
- Jin, Z.-H., Paulino, G. H., and Dodds, R. H., Jr. (2002). "Finite element investigation of quasistatic crack growth in functionally graded materials using a novel cohesive zone fracture model." *ASME J. Appl. Mech.*, 69, 370–379.
- Jin, Z.-H., Paulino, G. H., and Dodds, R. H., Jr. (2003). "Cohesive fracture modeling of elastic-plastic crack growth in functionally graded materials." *Eng. Fract. Mech.*, 70, 1885–1912.
- Kim, J.-H. (2003). "Mixed-mode crack propagation in functionally graded materials." PhD thesis, Univ. of Illinois at Urbana-Champaign, Urbana, Ill.
- Kim, J.-H., and Paulino, G. H. (2002a). "Finite element evaluation of mixed mode stress intensity factors in functionally graded materials." *Int. J. Numer. Methods Eng.*, 53, 1903–1935.
- Kim, J.-H., and Paulino, G. H. (2002b). "Isoparametric graded finite elements for nonhomogeneous isotropic and orthotropic materials." *ASME J. Appl. Mech.*, 69, 502–514.
- Kim, J.-H., and Paulino, G. H. (2003a). "Mixed-mode J-integral formulation and implementation using graded finite elements for fracture analysis of nonhomogeneous orthotropic materials." *Mech. Mater.*, 35, 107–128.
- Kim, J.-H., and Paulino, G. H. (2003b). "T-stress, mixed-mode stress intensity factors, and crack initiation angles in functionally graded materials: A unified approach using the interaction integral method." *Comput. Methods Appl. Mech. Eng.*, 192, 1463–1494.
- Kim, J.-H., and Paulino, G. H. (2003c). "The interaction integral for fracture of orthotropic functionally graded materials: Evaluation of stress intensity factors." *Int. J. Solids Struct.*, 40, 3967–4001.
- Kim, J.-H., and Paulino, G. H. (2003d). "An accurate scheme for mixed-mode fracture analysis of functionally graded materials using the interaction integral and micromechanics models." *Int. J. Numer. Methods Eng.*, 58, 1457–1497.
- Kim, J.-H., and Paulino, G. H. (2004). "T-stress in orthotropic functionally graded materials: Lekhnitskii and Stroh formalism." *Int. J. Fract.*, 126, 345–389.
- Kim, Y. J., Kim, H.-G., and Im, S. (2001). "Mode decomposition of three-dimensional mixed-mode cracks via two-state integrals." *Int. J. Solids Struct.*, 38, 6405–6426.
- Knowles, J. K., and Sternberg, E. (1972). "On a class of conservation laws in linearized and finite elastostatics." *Arch. Ration. Mech. Anal.*, 44, 187–211.
- Konda, N., and Erdogan, F. (1994). "The mixed-mode crack problem in a nonhomogeneous elastic medium." *Eng. Fract. Mech.*, 47, 533–545.
- Krysl, P., and Belytschko, T. (1999). "The element free Galerkin method for dynamic propagation of arbitrary 3-D cracks." *Int. J. Numer. Methods Eng.*, 44, 767–800.
- Li, C., and Zou, Z. (1998a). "Internally circumferentially cracked cylinders with functionally graded material properties." *Int. J. Pressure Vessels Piping*, 75, 499–507.
- Li, C., and Zou, Z. (1998b). "Stress intensity factors for a functionally graded material cylinder with an external circumferential crack." *Fatigue Fract. Eng. Mater. Struct.*, 21, 1447–1457.
- Li, C., Zou, Z., and Duan, Z. (1999). "Stress intensity factors for functionally graded solid cylinders." *Eng. Fract. Mech.*, 63, 735–749.
- Li, C., Zou, Z., and Duan, Z. (2000). "Multiple isoparametric finite element method for nonhomogeneous media." *Mech. Res. Commun.*, 27, 137–142.
- Nahta, R., and Moran, B. (1993). "Domain integrals for axisymmetric interface problems." *Int. J. Solids Struct.*, 30, 2027–2040.
- Nakamura, T. (1991). "Three-dimensional stress fields of elastic interface cracks." *ASME J. Appl. Mech.*, 58, 939–946.
- Nakamura, T., and Parks, D. M. (1989). "Antisymmetrical 3-D stress field near the crack front of a thin elastic plate." *Int. J. Solids Struct.*, 25, 1411–1426.
- Ozturk, M., and Erdogan, F. (1995). "An axisymmetric crack in bonded materials with a nonhomogeneous interfacial zone under torsion." *ASME J. Appl. Mech.*, 62, 116–125.
- Ozturk, M., and Erdogan, F. (1996). "Axisymmetric crack problem in bonded materials with a graded interfacial region." *Int. J. Solids Struct.*, 33, 193–219.
- Paulino, G. H., Jin, Z.-H., and Dodds, R. H., Jr. (2002). "Failure of functionally graded materials." *Comprehensive structural integrity*, Vol. 2, B. Karihaloo and W. G. Knauss, eds., Elsevier, New York.
- Paulino, G. H., and Kim, J.-H. (2004). "A new approach to compute

- T-stress in functionally graded materials using the interaction integral method." *Eng. Fract. Mech.*, 71, 1907–1950.
- Pook, L. P. (1994). "Some implications of corner point singularities." *Eng. Fract. Mech.*, 48, 367–378.
- Rangaraj, S., and Kokini, K. (2003). "Interface thermal fracture in functionally graded zirconia-mullite-bond coat alloy thermal barrier coatings." *Acta Mater.*, 51, 251–267.
- Rao, B. N., and Rahman, S. (2003). "Mesh-free analysis of cracks in isotropic functionally graded materials." *Eng. Fract. Mech.*, 70, 1–27.
- Rice, J. R. (1968). "A path independent integral and the approximate analysis of strain concentration by notches and cracks." *J. Appl. Mech.*, 35, 379–386.
- Shih, C. F., Moran, B., and Nakamura, T. (1986). "Energy release rate along a three-dimensional crack front in a thermally stressed body." *Int. J. Fract.*, 30, 79–102.
- Stern, M., Becker, E. B., and Dunham, R. S. (1976). "A contour integral computation of mixed-mode stress intensity factors." *Int. J. Fract.*, 12, 359–368.
- Suresh, S., and Mortensen, A. (1998). *Fundamentals of functionally graded materials*, Institute of Materials, London.
- Sutradhar, S., and Paulino, G. H. (2004). "Symmetric Galerkin boundary element computation of T -stress and stress intensity factors for mixed-mode cracks by the interaction integral method." *Eng. Anal. Boundary Elem.*, 28, 1335–1350.
- Walters, M. C., Paulino, G. H., and Dodds, R. H., Jr. (2004). "Stress intensity factors for surface cracks in functionally graded materials under mode-I thermomechanical loading." *Int. J. Solids Struct.*, 41, 1081–1118.
- Walters, M. C., Paulino, G. H., and Dodds, R. H., Jr. (2005). "Interaction integral procedures for 3-D curved cracks including surface tractions." *Eng. Fract. Mech.*, 72, 1635–1663.
- Wang, X. (2004). "Elastic T -stress solutions for penny-shaped cracks under tension and bending." *Eng. Fract. Mech.*, 71, 2283–2298.
- Wei, L. W., Edwards, L., and Fitzpatrick, M. E. (2002). "FE analysis of stresses and stress intensity factors of interfacial cracks in a CTS specimen." *Eng. Fract. Mech.*, 69, 85–90.
- Williams, M. L. (1957). "On the stress distribution at the base of a stationary crack." *ASME J. Appl. Mech.*, 24, 109–114.
- Yau, J. F., Wang, S. S., and Corten, H. T. (1980). "A mixed-mode crack analysis of isotropic solids using conservation laws of elasticity." *ASME J. Appl. Mech.*, 47, 335–341.